Nanocomposite Polymer Electrolytes by *In situ* Polymerization of Methyl Methacrylate: For Electrochemical Applications

Shahzada Ahmad,[1] S. A. Agnihotry,[1] Sharif Ahmad[2]

[1]*Electronic Materials Division, National Physical Laboratory, New Delhi 110012, India*
[2]*Materials Research Laboratory, Department of Chemistry, Jamia Millia Islamia, New Delhi 110025, India*

Received 28 April 2007; accepted 16 September 2007
DOI 10.1002/app.27507
Published online 26 November 2007 in Wiley InterScience (www.interscience.wiley.com).

ABSTRACT: Hybrid materials, which combine properties of organic–inorganic materials, are of profound interest owing to their unexpected synergistically derived properties and are considered as innovative advanced materials promising new applications in many fields such as optics, electronics, ionics and mechanics. Inorganic fillers are added to polymers in order to increase some of the properties of the compounds. These hybrid polymeric materials are replacing the pristine polymers due to their higher strength and stiffness. In the present work, studies concerning the preparation of poly (methylmethacrylate) [PMMA] and the nanocomposites PMMA/SiO_2, PMMA/TiO_2 are reported. These nanocomposite polymers were synthesized by means of free radical polymerization of methylmethacrylate, further ''sol–gel'' transformation-based hydrolysis and condensation of corresponding alkoxide was used to prepare the inorganic phase during the polymerization process of MMA. Electrolytes were synthesized based on these nanocomposite polymers and have shown superior properties as compared to conventional polymer electrolytes. The nanocomposites and the nanocomposite polymer electrolytes (NPEs) with different lithium salts were investigated through an array of techniques including FTIR and calorimetry along with the electrochemical and rheological techniques. © 2007 Wiley Periodicals, Inc. J Appl Polym Sci 107: 3042–3048, 2008

Key words: nanocomposites; FTIR; *insitu* polymerization; polymer electrolytes

INTRODUCTION

Polymers, which have innumerable applications in diverse fields of life, can be further modified according to modern hi-tech application. Organic–inorganic nanocomposites are a versatile class of materials having enormous application potential, due to their tailorable mechanical, optical and electrical properties.[1–3] In the age of modern era multifunctional hybrid polymeric materials, which consist of organic and inorganic components, are replacing conventional polymers. These are often called polymer composites and offer improved properties including higher strength and stiffness than pristine polymers.[4,5] Different types of organic constituents or monomers can be used and various methods can be performed according to requirement. Nanocomposite polymers (NCPs) are polymers, which have dispersed phase in it with ultra fine dimension typically of some nanometer.[6] The choice of the polymer and dispersed phase is determined by the properties required for the end product. These nanocomposites exhibit enhanced thermal and dimensional stability, stiffness, strength, low thermal expansion and fire retardancy and also unusual magnetic, optical, electronic properties than their counterpart.[7–9] Nanoscale composite materials containing titanium oxide are interesting because of their potential applications in optoelectronic devices.[10,11] A great deal of research effort has been focused on both, synthesis of high quality transparent films consisting of polymer–TiO_2 hybrid nanocomposites and their linear optical properties.[12,13] Recently, the nonlinear optical properties of such materials have also received attention.

There are three common approaches for the synthesis of polymer nanocomposites, which have been adopted so far.[2,6] The first approach is the *insitu* polymerization technique, second is by dissolving the polymer in a solvent and then mixing with the dispersing media, while the third approach is of melt intercalation and involves heating the polymer above its glass transition temperature and then mixing with the dispersing medium. The first approach is rather simple and largely favored, as it neither requires the costly solvent nor does it consume energy and is very economical. In efforts for studying the behavior of polymer electrolytes for their possible applications in various electrochemical

Correspondence to: S. Ahmad (sahmad@mail.nplindia.ernet.in).
Contract grant sponsor: CSIR.

devices and in particular for secondary Li^+ batteries, recently these materials have attracted interest.[14–17] The approach is rather simple and facile than the earlier approach of mixing the nanoparticles in the polymer electrolytes. Among all other existing polymer materials, PMMA is well known as a glassy polymer and engineering plastic with a range of applications. It is also of special interest for us due to its amorphous nature and transparency along with a wide choice of carbonate solvents. Because of its amorphous nature, high dielectric constant and ambient temperature conductivity can be achieved in electrolytes based on it, which is not exhibited by other polymers. PMMA-based electrolytes are also the best candidates in electrochromic devices and sensors where transparency is a major prerequisite.

In our earlier communications, we have demonstrated the effect of nanosized SiO_2, TiO_2 addition in polymer electrolytes on conductivity,[18,19] as well as thermal and rheological properties. This motivated us to attempt a new route in which nano scale ceramic particles are precipitated in the polymer host. A simple method namely ''Sol–gel'' was followed for the same.[20–22] In this approach, free radical suspension polymerization in water medium with *insitu* ''Sol–gel'' transformation is used to prepare an amorphous PMMA–SiO_2, PMMA–TiO_2 nanocomposite polymer.

Finally these NCPs are encaged in a liquid electrolyte, composed of the lithium salts series of nitrogen family i.e. Lithium Imide and LiBETI in an aprotic solvent PC. LiBETI is of profound interest for battery application due to its thermal stability and uncorrosive behavior with aluminum anode, which is a major current collector in lithium battery. The detailed analysis of our preliminary investigations on thermal, electrochemical, rheological, and spectroscopic study is given herewith.

EXPERIMENTAL

Materials

Methyl methacrylate (was made inhibitor free by passing through activated alumina column or by vacuum distillation), Propylene carbonate are of synthesis grade, ethyl alcohol and hydrochloric acid (37%) all were supplied by Merck, Germany. Tetraethyl orthosilicate (TEOS) and Titanium (IV) isopropoxide used as precursors for the inorganic fillers and were obtained from Aldrich. Benzoyl peroxide, [BPO] (Loba chemicals, India) used as an initiator while Poly vinyl alcohol (Aldrich) and anhydrous disodium hydrogen phosphate (CDH, India) were used as received. Lithium Imide (LiIm) and Lithium BETI (LiBETI) salts were kindly supplied by 3M and were vacuum dried at 120°C overnight before use.

Synthesis of Polymer

A typical procedure to prepare PMMA was followed which involved placing 20 mL of MMA, 0.15 g (0.75%) of BPO in 100 mL of water and 0.5 g of PVA and 5 g of disodium hydrogen phosphate in a 250-mL three-necked round bottom flask and then refluxing for 1 h at 80°C under vigorous stirring. Nitrogen was bubbled into the flask throughout the reaction. The solution was then filtered, washed, and finally dried at 100°C for 24 h under vacuum to yield the PMMA solid material.

Synthesis of PMMA–SiO_2 and PMMA–TiO_2 composites

The same procedure was followed except after half on hour of reaction the sol was added. SiO_2-based sol was prepared by taking TEOS (2.0 mL), deionized water (0.4 mL) and HCl (0.04 mL, used to catalyze the hydrolysis) was mixed in a beaker and pre hydrolyzed in air and then it was sonicated for 15 min. to facilitate the conversion of ethoxy ligands to Si—OH groups. The TiO_2-based sol was prepared using titanium isopropoxide (Ti-iP), deionized water, ethanol and hydrochloric acid, according to the method described elsewhere.[22,23] Ti-iP (2 mL) was first mixed with ethanol (20 mL) in a beaker and stirred for 30 min. A mixture of deionized water and HCl was poured under stirring into the transparent solution to promote hydrolysis. The Ti-iP concentration in the solution was fixed at 0.4*M* with an under stoichiometric ratio of water to Ti-iP (rw) of 0.82, and the pH value of 1.3 was used to obtain a stable solution (i.e. with longest gelation time). Furthermore, this homogeneous mixture was added drop wise over 30 min into the reaction media of monomers with rigorous stirring to avoid local inhomogenities.

Electrolyte preparation

An appropriate amount of LiIm or LiBETI salts were first dissolved in PC to result in a 1*M* liquid electrolyte. The chosen concentration (1*M*) in addition to the highest ionic conductivity is characterized by negligible ion pair formation in the liquid electrolyte. In the obtained liquid electrolyte 15 wt % of PMMA or PMMA–SiO_2 or PMMA–TiO_2 was then added slowly while heating at 55°C for 2 h until transparent NPEs were obtained. A total of six samples were prepared in a glove box under argon atmosphere from the above three composition with two different lithium salts.

Instrumentation

Electrolyte conductivities were measured using Metrohm 712 Conductometer, having a cell constant, K

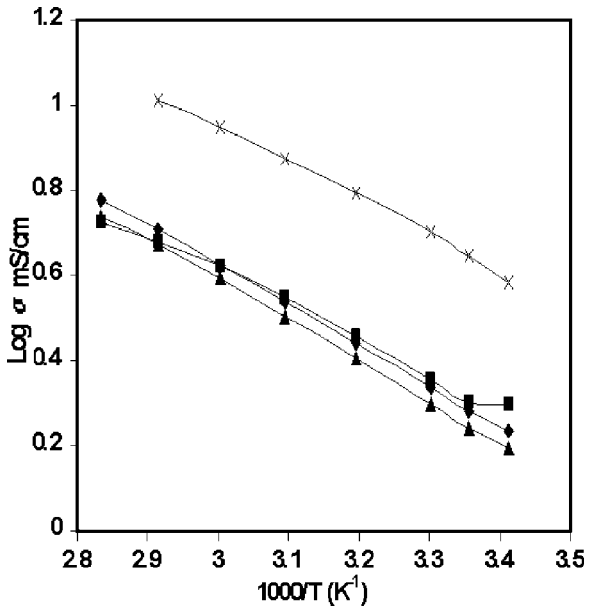

Figure 1 Arrhenius plots of conductivity with liquid electrolyte 1*M* (×), and PMMA (◆), PMMA-SiO_2 (■), and PMMA-TiO_2 (▲) based electrolytes with LiBETI salt.

0.89 cm^{-1} and controlled by a Paar Physica circulating water bath. Rheological measurements were carried out on Anton-Paar DV2P digital viscometer equipped with a temperature controlled circulating water bath at a shear rate 0.17–68 s^{-1}. Differential scanning calorimetry (DSC) was performed on a Mettler Toledo analyzer that consists of a DSC 851 main unit and STARe software equipped with a low temperature cell under nitrogen purge and the samples were heated to 400°C at a rate of 10°C/min. Infrared spectra were recorded in the region of 4000–400 cm^{-1} on a computer interfaced Perkin-Elmer FX-RX1 between NaCl windows. Cyclic voltametry was performed on Omni 90 Potentiostat, Cypress systems using a computer controlled software at a scan rate of 20 mV s^{-1}.

RESULT AND DISCUSSIONS

Conductivity measurements

Figure 1 depicts the Arrhenius plots of conductivity of the synthesized electrolytes. Liquid electrolyte consisting of 1*M* LiBETI in PC exhibits maximum conductivity (4.43 mS/cm) at room temperature than the rest of the systems. It can be seen that the addition of polymer and its composite brings down conductivity marginally and without obstacle the motion of ions to a large extent from that in the liquid electrolyte. The SiO_2-based electrolytes exhibit higher conductivity than the pristine polymer and TiO_2-based electrolytes, due to the less aggregation, ion pair formation as discussed in detail in FTIR section. The ambient temperature conductivity values are 1.92 mS/cm for pristine polymer electrolyte, 2.02 mS/cm for SiO_2-based and 1.74 for TiO_2-based electrolytes. The increase in conductivity from PMMA to PMMA–SiO_2-based system is also due to the increase in segmental motion of the polymer,[17,24] as the glass transition temperatures (T_g) decreases from polymer to NPEs discussed in more detail in the calorimetry section.

In order to further investigate the conduction mechanism the activation energy (E_a) was calculated in a similar fashion as by other workers[24,25] by fitting the conductivity in the following VTF equation since the curved profile are non-Arrhenius in nature.

$$\sigma T^{1/2} = A \exp(-B/T - T_o) \quad (1)$$

Here A is related to charge concentration, T_o is ideal glass transition temperature and here taken as T_g in Kelvin determined by DSC measurements, while B is proportional to activation energy of conduction and its product with gas constant (R) gives E_a. Both the parameters were obtained by best fitting the curve and were found to be better than 0.05.

The calculated activation energy is 4.8 kJ/mole for polymer electrolyte, 4.19 and 5.15 kJ/mole for PMMA–SiO_2 and PMMA–TiO_2-based electrolytes, respectively. The slight increase in the conductivity for SiO_2-based electrolytes can be attributed to the presence of the well dispersed fillers in the matrix besides the intercalated ones. The fillers may help to dissociate the lithium salts more easily and thus provide more free lithium cations. The lower the activation energy the greater will be ionic conductivity.

Figure 2 depicts the Arrhenius plots of conductivity for LiIm salt-based systems and exhibits non-

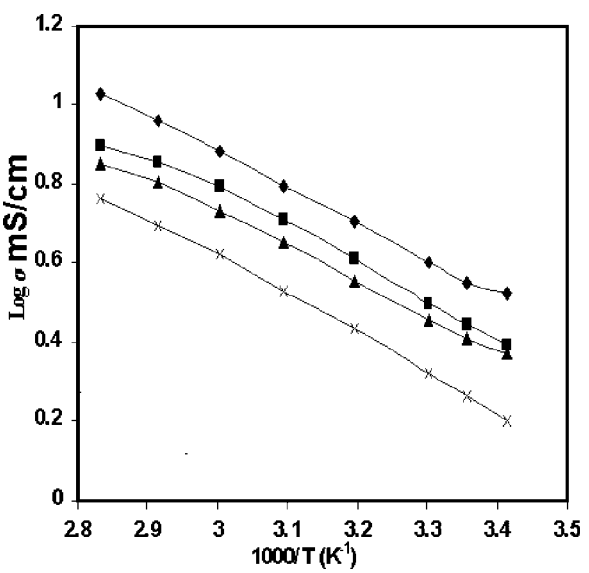

Figure 2 Arrhenius plots of conductivity with liquid electrolyte (◆), and PMMA (■), PMMA-SiO_2 (▲), and PMMA-TiO_2 (×) based electrolytes with LiIm salt.

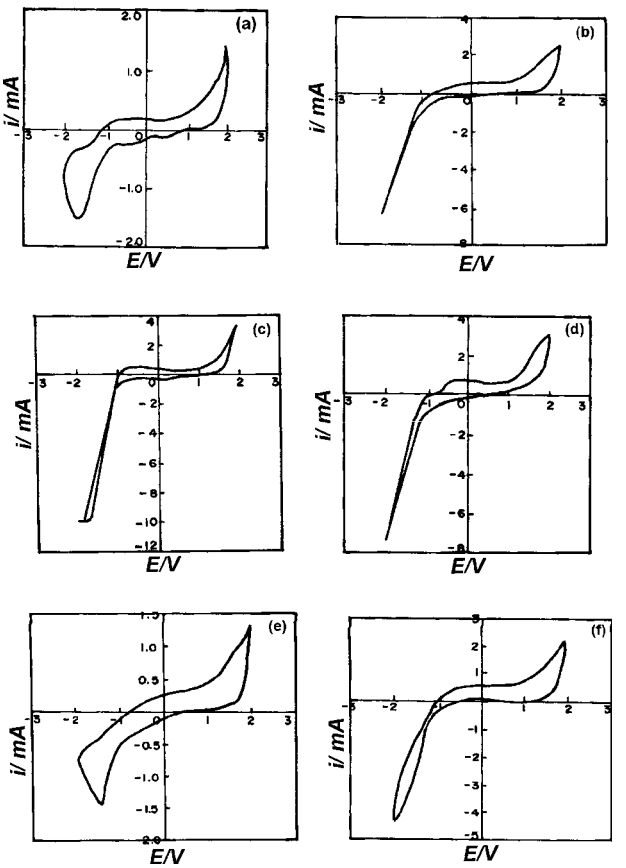

Figure 3 Cyclic voltammogram of (a) PMMA, (c) PMMA-SiO_2, and (e) PMMA–TiO_2-based electrolytes with LiIm and (b), (d), (f) with LiBETI salts, respectively.

Arrhenius behavior. The highest ionic conductivity shown by 1*M* liquid electrolytes in PC with value at 3.55 mS/cm, followed by GPE 2.81 mS/cm, while NPEs based on PMMA–SiO_2 and PMMA–TiO_2 exhibit ionic conductivity values of 2.59 mS/cm and 1.83 mS/cm, respectively, at 25°C. It is worth mentioning here that the decrease in conductivity from liquid to GPE is to lesser extent in LiIm than in LiBETI-based polymer electrolytes, which may be due to the bulky ethyl group present in the LiBETI salt and further investigations are necessary to explore the mechanism and establish a correlation.

Voltammetry

In order to study the electrochemical stability limits of electrolytes i.e. the potential where electrolytes oxidation and reduction start, cyclic voltammetry was used. The electrochemical behavior in a voltage range of ±2V was studied. Platinum has the largest current densities, indicating its suitability for stability measurements and also due to its rapid kinetics and no interfering reaction. Figure 3 illustrates the voltammograms, which were obtained by using two electrodes as counter and working electrodes both of Platinum, while Ag/AgCl was used as the reference electrode. In the experimental voltage range, any significant oxidation and reduction peak cannot be observed. This is in well accordance with the other author's report that the synthesized electrolyte is water and moisture free.[26] The cathodic and anodic current maxima are very nearer to each other, this shows the reversibility of the electrolytes. The traces are reproducible upto the studied 20th cycle (not shown here) and no degradation can be observed. The PMMA–SiO_2-based electrolytes show higher value of current for both the salts due to the hydrophobic nature of SiO_2 particles. All the voltammograms are identical in shape except the TiO_2-based electrolytes in which the cathodic peak is the characteristic of TiO_2 particles.[27]

An improvement in the kinetics can be concluded due to the presence of filler particles as indicated by the better resolved peak and high current response obvious from the voltammograms.

Viscosity

Arrhenius plots of viscosity are illustrated in Figure 4 and these profiles are seen to exhibit non-Arrhenius behavior. The viscosity increases for NPEs from the pristine electrolyte. The TiO_2-based electrolyte exhibits maximum viscosity followed by SiO_2 and then by PMMA-based electrolytes. The increase in the viscosity is only by a factor with its value at 25°C for PMMA–TiO_2 (14.1 Pa s) and for PMMA–SiO_2 (8.5 Pa s) while for PMMA-based electrolytes it is 5.8 Pa s. The higher viscosity of NPEs points towards the intercalation of nanoparticles in the polymer matrix, resulting in a higher mechanical integrity in the NPEs.[1]

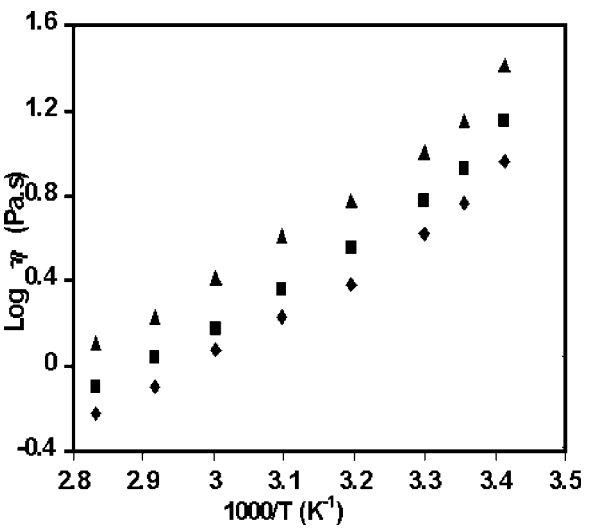

Figure 4 Arrhenius plots of viscosity with PMMA (◆), PMMA–SiO_2 (■), and PMMA–TiO_2 (▲) based electrolytes.

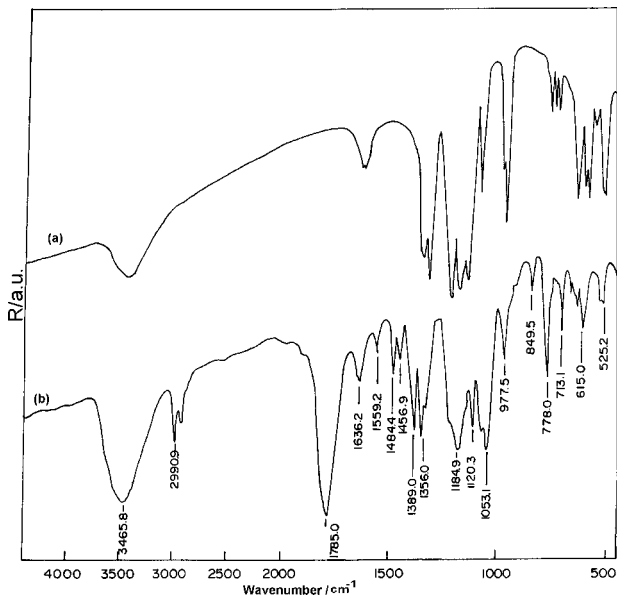

Figure 5 FTIR spectra of (a) LiBETI salt and (b) 1*M* LiBETI-PC liquid electrolyte.

Spectral studies

FTIR spectra of LiBETI salt and the corresponding liquid electrolyte compromising 1*M* LiBETI in PC are illustrated in Figure 5. In the spectrum of LIBETI the bands at 3443 and 1635 are due to ν(OH) and δ(OH), respectively, while the bands at 1354 and 1328.8 cm^{-1} are due to ν_a (SO_2) in plane and out plane bending, respectively. The ν_{as} modes of SO_2 appear at 1224, 998, and 981 cm^{-1} and $\nu_s(SO_2)$ appears at 1148.7 and its bending deformational modes appear at 617 and 602 cm^{-1}.

The symmetric CF_2 stretching band is at 1184.6 cm^{-1} and the bands at 1096.7, 743, 570, and 527 cm^{-1} are the various vibrational modes of CF_3.[28] The bands due to ν_s(SNS) and ν(C—S) modes are at 776.7 and 768 cm^{-1}, respectively. The Figure 5(b) shows the various vibrational modes and characteristic infrared frequencies of PC along with the bands of LiBETI, the former has already been summarized by Battisti et al. in more detail.[29] Therefore an indepth and intricate analysis of the various PC bands is considered as unnecessary to be discussed and assigned, and all the bands are well in accordance with their results. The fingerprint characteristic vibration bands of PMMA appear at 1727 ν(C=O), 1450 ν(C—O). The bands at 3000 and 2900 cm^{-1} correspond to the C—H stretching of the methyl group (CH_3) while the bands at 1300 and 1450 cm^{-1} are associated with C—H symmetric and asymmetric stretching modes, respectively. The 1240 cm^{-1} band is assigned to torsion of the methylene group (CH_2) and the 1150 cm^{-1} band corresponds to vibration of the ester group C—O while C—C stretching bands are at 1000 and 800 cm^{-1}. The fingerprint frequencies of SiO_2 are 464, 800, 950, and 1086.5 cm^{-1}, respectively, due to Si—O—Si bending, symmetric Si—O—Si stretching, Si—OH flexible vibration and asymmetric Si—O—Si stretching vibration modes.[30] The peaks in the region at 910–960 cm^{-1} is due to the overlapping from vibrations of Si—OH bonds.[31,32]

The broad and weak peaks in the PMMA spectrum are highly intense and sharp in the PMMA–TiO_2 spectrum. This latter feature can be explained due to superposition of the ν(OH) mode of interacting H-bonds and the symmetric and antisymmetric ν(OH) mode of molecular water coordinated to Ti^{4+} cations. The signature band of ν(Ti—O) vibration appears at 820 cm^{-1} which is very near to a band at 827cm^{-1} due to C—C stretching of PMMA.[22,33]

The FTIR spectra of polymer electrolytes were also recorded and no significant changes have been observed; however, there is extensive overlapping of the bands. The characteristic bands of Si—O and even Ti—O disappear in the spectra of electrolytes due to the number of constituents present in them. The Figure 6 shows no significant wavenumber shift, broadening or splitting in the five characteristics peaks of LiBETI. The bands corresponding to asymmetric stretching mode of (SNS) appears at 1054.4

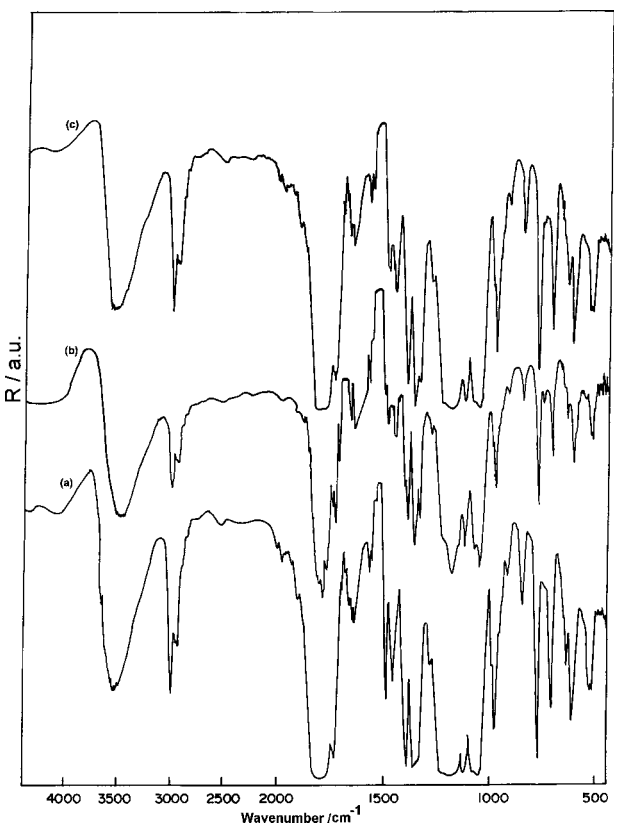

Figure 6 FTIR spectra of (a) PMMA, (b) PMMA- SiO_2, (c) PMMA–TiO_2-based polymer electrolytes with LiBETI salt.

cm^{-1} for the GPE sample is shifted to 1052.8 and 1053.3 cm^{-1} for PMMA–SiO_2 and PMMA–TiO_2-based electrolytes, respectively. Similar changes can be observed for asymmetric stretching mode of (SO_2) which appears at 1339, 1332.7, 1327 cm^{-1} for PMMA, PMMA–SiO_2 and PMMA–TiO_2 electrolytes, respectively, due to the reduction in the ion pair formation induced by the fillers. The band due to C=O stretching mode of PC shows downward shift due to H-bonding with the filler particles and appears at 1793.4, 1786.3, 1782.4, respectively, for the samples in the same sequence as above, while the band corresponding to C=O stretching mode of PMMA remains unperturbed and lies around 1731 cm^{-1}.

The ν(C—O) mode of the (—COO—) group of PMMA, which appears at 1274 cm^{-1} in pure PMMA appears here at 1260 cm^{-1} for PMMA and at 1271.5 cm^{-1} for both the electrolytes, respectively, due to their association with the filler. In the low frequency region a band appears at 464 cm^{-1} in the PMMA–SiO_2-based electrolytes, which characterizes symmetric stretching mode of Si—O—Si band, is absent in the rest of the systems. Since the degree of ion pairing is very less in LiBETI-based electrolytes, so no noticeable changes can be observed in moving from polymer to NPEs and this is in good agreement with other author's FTIR as well as Raman spectroscopic data. The bands, which appear at 1553, 1451, 1390, 1355, 1337, 1181.5, 1120, 1054, 920, 849.7, 778, 713, 640 cm^{-1} are due to various vibrational modes of PC[29]; similarly the rest of the bands belong to lithium salt and PMMA as assigned earlier.[34]

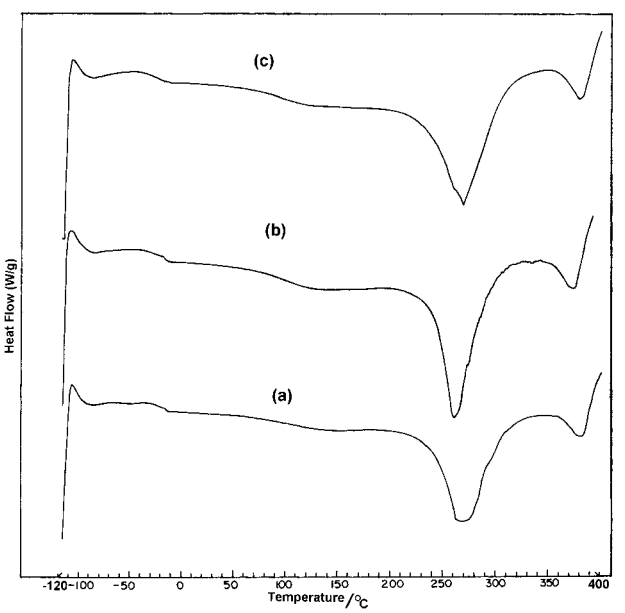

Figure 7 DSC profiles of (a) PMMA, (b) PMMA–SiO_2, (c) PMMA–TiO_2-based polymer electrolytes with LiBETI salt.

TABLE I
Thermal Properties of the Synthesized Electrolytes with LiBETI Salt

Electrolytes	T_g (°C)	T_{m1}(°C)	T_{m2} (°C)
PMMA	−109.9	270	380.5
PMMA–SiO_2	−114.7	270	381.5
PMMA–TiO_2	−116	270.5	380

T_{m1}, first melting temperature, T_{m2}, second melting temperature.

Calorimetry Studies

The thermograms of the synthesized electrolytes for LiBETI salt have been illustrated in Figure 7. The glass transition temperatures (T_g) decrease in going over from polymer electrolytes to nanocomposite electrolytes as shown in Table I. The T_g is directly related to the flexibility of the polymer chains, so it can be concluded that the formation of nanocomposite has induced more flexibility in the polymer chain. The T_g lies in the order of PMMA > PMMA–SiO_2 > PMMA–TiO_2. *In situ* prepared nanoparticles form hydrogen bonding between the surface —OH groups and with the C=O of MMA. Such H-bonds skew the polymer chains and result in additional free volume. It appears that this irregular chain- folding effect perturbs the bulk of polymer phase and causes reduction in the matrix density, resulting in a higher local mobility for the polymer segments. The thermograms display no other peak upto 250°C but two endothermic peaks appear there after. Because of the high thermal stability of LiBETI salt and complete solvation in the PC solvent, the solvent evaporation peak has also shifted to higher temperature than reported earlier.[18] The first endothermic peak is due to evaporation of PC as its melting point is 236°C and is shifted to higher temperature (270°C) and remains almost unaffected for all the electrolytes under considerations. The second peak which lies at around 380°C for PMMA and 381.5°C for PMMA–SiO_2 system is due to the degradation of unsaturated groups of PMMA and also due to the conversion in the monomer. This result is well in accordance with the other workers[35,36] that addition of nanosilica particles into the PMMA did not significantly alter the thermal degradation mechanism of the polymer i.e. the thermal stability of PMMA was not enhanced with the addition of silica particles.

CONCLUSIONS

An experimental protocol has been shown to synthesize PMMA, PMMA–SiO_2 and PMMA–TiO_2 nanocomposites. These nanocomposites were synthesized via sol–gel transformation in an *insitu* free radical polymerization of MMA. Thermal and FTIR studies

support the formation of nanocomposite. Finally these NCPs were encaged in liquid electrolytes comprising LiIm and LiBETI salts. The properties of these materials are even better than pure polymer as silica clusters induce structural disorder which favor more ionic path and the glass transition temperatures (T_g) are seen to decrease in going from polymer electrolytes to nanocomposite polymer electrolytes pointing towards more flexibility in the polymer chain, which has also been established by its activation energy. The conductivity values do not change to a larger extent but these nanocomposites impart better mechanical properties to the polymer electrolytes. Because of the number of constituents present in these NPE samples, the FTIR spectra do not give a clear picture of the local environment and the interactions between them.

We believe that these NPEs, due to their merits are suitable candidates particularly for polymer electrolytes and experiments are underway to incorporate it in a device and study its behavior in electrochromic devices.

One of the authors, S. A. acknowledges CSIR for financial support and the authors profusely thank Dr. S. K. Dhawan for DSC measurements and Dr. S. T. Lakshmikumar and Dr. M. Deepa for necessary help. The authors are grateful to the 3M for their generosity for providing us Li imide and LiBETI salts.

References

1. Meneghetti, P.; Qutubuddin, S. Langmuir 2004, 20, 3424.
2. Ahmadi, S. J.; Huang, Y. D.; Li, W. J Mater Sci 2004, 39, 1919.
3. Aymonier, C.; Bortzmeyer, D.; Thomann, R.; Mulhaupt, R. Chem Mater 2003, 15, 4874.
4. Mark, J. E. Polym Eng Sci 1996, 36, 2905.
5. Giannelis, E. P. Adv Mater 1996, 8, 29.
6. Qutubuddin, S.; Fu, X. In: Nano Surface Chemistry; Rosoff, M., Eds.; Marcel Dekker: New York, 2002; p 653.
7. Qiang, X.; Chunfang, Z.; Zun, Y. J.; Yuan, C. S. J Appl Polym Sci 2004, 91, 2739.
8. Avella, M.; Errico, M. E.; Martelli, S.; Martuscelli, E. Appl Organomet Chem 2001, 15, 435.
9. Wang, H. W.; Shieh, C. F.; Chang, K. C.; Chu, H. C. J Appl Polym Sci 2005, 97, 2175.
10. Du, G. H.; Chen, Q.; Che, R. C.; Yuan, Z. Y.; Peng, L. M. Appl Phys Lett 2001, 79, 3702.
11. Suzuki, N.; Tomita, Y.; Kojima, T. Appl Phys Lett 2002, 81, 4121.
12. Lee, L.; Chen, W. C. Chem Mater 2001, 13, 1137.
13. Zhang, J.; Wang, B.; Ju, X.; Liu, T.; Hu, T. Polymer 2001, 42, 3697.
14. Agnihotry, S. A.; Ahmad, S.; Gupta, D.; Ahmad, S. Electrochim Acta 2004, 49, 2343.
15. Bronstein, L. M.; Ashcraft, Desanto, P., Jr.; Karlinsey, R. L.; Zwanziger, J. W. J Phys Chem B 2004, 108, 5851.
16. Karlinsey, R. L.; Bronstein, L. M.; Zwanziger, J. W. J Phys Chem B 2004, 108, 918.
17. Liu, Y.; Lee, J. Y.; Hong, L. J Power Sources 2004, 129, 303.
18. Ahmad, S.; Bohidar, H. B.; Ahmad, S.; Agnihotry, S. A. Polymer 2006, 47, 3583.
19. Ahmad, S.; Ahmad, S.; Agnihotry, S. A. J Power Sources 2006, 159, 205.
20. Limmer, S. J.; Seraji, S.; Wu, Y.; Chou, T. P.; Nguyen, C.; Cao, G. Adv Funct Mater 2002, 12, 59.
21. Schmidt, H. J Non-Cryst Solids 1988, 100, 51.
22. Ahmad, S.; Ahmad, S.; Agnihotry, S. A. Bull Mater Sci 2007, 30, 31.
23. Burgos, M.; Langlet, M. J Sol–Gel Sci Technol 1999, 16, 267.
24. Bohnke, O.; Frand, G.; Rezrazi, M.; Rousselot, C.; Truche, C. Solid State Ionics 1993, 66, 105.
25. Meneghetti, P.; Qutubuddin, S.; Webber, A. Electrochim Acta 2004, 49, 4923.
26. Joho, F.; Rykart, B.; Imhof, R.; Novak, P.; Spahr, M. E.; Monnier, A. J Power Sources 1999, 81/82, 243.
27. Georen, P.; Lindbergh, G. J Power Sources 2003, 124, 213.
28. Ota, H.; Sakata, Y.; Wang, X.; Sasahara, J.; Yasukawa, E. J Electrochem Soc 2004, 151, A 437.
29. Battisti, D.; Nazri, G.; Kalssen, B.; Aroca, R. J Phys Chem 1993, 97, 5826.
30. Hwang, S. T.; Hahn, Y. B.; Nahm, K. S.; Lee, Y. S. Colloids Surf A Physicochem Eng Aspects 2005, 259, 63.
31. Baraton, M. I. In Handbook of Nanostructured Materials and Nanotechnology; Nalwa, H. S., Eds.; Academic Press: New York, 2004; Vol. 2, p 90.
32. Jung, K. Y.; Park, S. B. Appl Catal B Environ 2000, 25, 249.
33. Maira, A. J.; Coronado, J. M.; Augugliaro, V.; Yeung, K. L.; Conesa, J. C.; Soria, J. J Catal 2001, 202, 413.
34. Deepa, M.; Agnihotry, S. A.; Gupta, D.; Chandra, R. Electrochim Acta 2004, 49, 373.
35. Kashiwagi, T.; Morgan, A. B.; Antonucci, J. M.; VanLandingham, M. R.; Harris, R. H.; Awad, W. H. J Appl Polym Sci 2003, 89, 2072.
36. Liu, Y. L.; Hsu, C. Y.; Hsu, K. Y. Polymer 2005, 46, 1851.